PHYSICAL REVIEW E **95**, 061201(R) (2017)

Energy transfer channels and turbulence cascade in Vlasov-Maxwell turbulence

Yan Yang,[1,2] W. H. Matthaeus,[2] T. N. Parashar,[2] P. Wu,[2,3] M. Wan,[4] Y. Shi,[1] S. Chen,[1,4] V. Roytershteyn,[5] and W. Daughton[6]

[1]*State Key Laboratory for Turbulence and Complex Systems, Center for Applied Physics and Technology, College of Engineering, Peking University, Beijing 100871, China*

[2]*Bartol Research Institute and Department of Physics and Astronomy, University of Delaware, Newark, Delaware 19716, USA*

[3]*School of Mathematics and Physics, Queen's University Belfast, BT7 1NN, United Kingdom*

[4]*Department of Mechanics and Aerospace Engineering, South University of Science and Technology of China, Shenzhen, Guangdong 518055, China*

[5]*Space Science Institute, Boulder Colorado 80301, USA*

[6]*Los Alamos National Laboratory, Los Alamos, New Mexico 87545, USA*

(Received 30 January 2017; revised manuscript received 28 March 2017; published 29 June 2017)

Analysis of the Vlasov-Maxwell equations from the perspective of turbulence cascade clarifies the role of electromagnetic work, and reveals the importance of the pressure-strain relation in generating internal energy. Particle-in-cell simulation demonstrates the relative importance of the several energy exchange terms, indicating that the traceless pressure-strain interaction "*Pi-D*" is of particular importance for both electrons and protons. The *Pi-D* interaction and the second tensor invariants of the strain are highly localized in similar spatial regions, indicating that energy transfer occurs preferentially in coherent structures. The collisionless turbulence cascade may be fruitfully explored by study of these energy transfer channels, in addition to examining transfer across spatial scales.

DOI: 10.1103/PhysRevE.95.061201

Introduction. Turbulence is characterized by the transfer of energy from large to small scales where dissipation occurs. This *cascade* process, fundamental in hydrodynamics [1], magnetohydrodynamics [2], and fluid plasma models [3], may be analyzed using phenomenological approaches [4], scale-to-scale transfer [5,6], and rigorous third order laws [7–9]. Here we are concerned with the nature of cascade in collisionless plasmas, especially at scales in which kinetic processes dominate [10]. The collisionless cascade has been studied in various simplified approaches, such as spectral phenomenologies [11,12] and gyrokinetic approximations [13,14]. Fourier scale filtering has been employed to study the electrostatic "free energy" cascade [15] in gyrokinetics, and associated numerical models [16]. Other simplifications assume that linear modes, e.g., kinetic Alfvén waves or whistler modes [12,17–19], dominate the nonlinear couplings. Here we adopt a different approach in which we analyze ideal energy transfer in the full Vlasov-Maxwell system, without reliance on specific mechanisms, modes, or fluid simplifications. This Rapid Communication begins such study by identifying the relevant channels of energy transfer. Using kinetic plasma simulation, we evaluate the relative strength of these transfer channels and demonstrate their concentration in spatial coherent structures. This provides a perspective of cascade and dissipation, without the need to select specific dissipative processes.

Energy balance. The mean-field velocity distribution $f = f(\boldsymbol{x},\boldsymbol{v},t)$ of the plasma species α, with mass m_α, depends on position $\boldsymbol{x}$, velocity $\boldsymbol{v}$, and time t, and obeys the Vlasov equation

$$\partial_t f_\alpha + \boldsymbol{v}\cdot\nabla f_\alpha + \frac{\mathbf{F}}{m_\alpha}\cdot\nabla_{\boldsymbol{v}} f_\alpha = 0. \tag{1}$$

Absent external forces, the force on particles with charge q_α is $\mathbf{F} = q_\alpha[\boldsymbol{E} + (\boldsymbol{v}/c \times \boldsymbol{B})]$, with $\boldsymbol{E}$ and $\boldsymbol{B}$ determined by Maxwell's equations. The sources for electric field $\boldsymbol{E}$ and magnetic field $\boldsymbol{B}$ are the charge density ρ and (total) electric current density $\boldsymbol{j}$.

The number density of species α is $n_\alpha = \int f_\alpha(\boldsymbol{x},\boldsymbol{v},t)d\boldsymbol{v}$, while the corresponding total kinetic energy is $\mathcal{E}_\alpha = \frac{1}{2}m_\alpha \int \boldsymbol{v}^2 f_\alpha(\boldsymbol{x},\boldsymbol{v},t)d\boldsymbol{v}$. The first two velocity space moments of the Vlasov equation are a continuity equation $\partial_t\rho_\alpha + \nabla\cdot(\rho_\alpha\boldsymbol{u}_\alpha) = 0$, and a momentum equation $\partial_t(\rho_\alpha\boldsymbol{u}_\alpha) + \nabla\cdot(\rho_\alpha\boldsymbol{u}_\alpha\boldsymbol{u}_\alpha) = -\nabla\cdot\boldsymbol{P}_\alpha + n_\alpha q_\alpha(\boldsymbol{E} + \boldsymbol{u}_\alpha/c \times \boldsymbol{B})$, for each species α. The time rate of change of the total kinetic energy in the species α obeys [20,21]

$$\partial_t\mathcal{E}_\alpha + \nabla\cdot(\mathcal{E}_\alpha\boldsymbol{u}_\alpha + \boldsymbol{P}_\alpha\cdot\boldsymbol{u}_\alpha + \boldsymbol{h}_\alpha) = n_\alpha q_\alpha\boldsymbol{u}_\alpha\cdot\boldsymbol{E}. \tag{2}$$

In the above expressions, the mass density is $\rho_\alpha = m_\alpha n_\alpha$, the fluid flow (bulk) velocity is $\boldsymbol{u}_\alpha = n_\alpha^{-1}\int \boldsymbol{v} f_\alpha(\boldsymbol{x},\boldsymbol{v},t)\,d\boldsymbol{v}$, the pressure tensor is $\boldsymbol{P}_\alpha = m_\alpha\int(\boldsymbol{v}-\boldsymbol{u}_\alpha)(\boldsymbol{v}-\boldsymbol{u}_\alpha) f_\alpha(\boldsymbol{x},\boldsymbol{v},t)d\boldsymbol{v}$, and the heat flux vector is $\boldsymbol{h}_\alpha = \frac{1}{2}m_\alpha\int(\boldsymbol{v}-\boldsymbol{u}_\alpha)^2(\boldsymbol{v}-\boldsymbol{u}_\alpha)f_\alpha(\boldsymbol{x},\boldsymbol{v},t)d\boldsymbol{v}$, each of these for the species α.

Decomposing the total energy $\mathcal{E}_\alpha$ into average and random parts facilitates the understanding of heating processes. On defining the fluid kinetic energy of species α as $E_\alpha^f = \frac{1}{2}\rho_\alpha\boldsymbol{u}_\alpha^2$ and the thermal (random) energy as $E_\alpha^{\rm th} = \frac{1}{2}m_\alpha\int(\boldsymbol{v}-\boldsymbol{u}_\alpha)^2 f_\alpha(\boldsymbol{x},\boldsymbol{v},t)d\boldsymbol{v}$, it is evident that $\mathcal{E}_\alpha = E_\alpha^f + E_\alpha^{\rm th}$. Multiplying the momentum equation by $\boldsymbol{u}_\alpha$ results in the fluid flow energy equation:

$$\begin{aligned}\partial_t E_\alpha^f + \nabla\cdot\left(E_\alpha^f\boldsymbol{u}_\alpha + \boldsymbol{P}_\alpha\cdot\boldsymbol{u}_\alpha\right)\\ = (\boldsymbol{P}_\alpha\cdot\nabla)\cdot\boldsymbol{u}_\alpha + n_\alpha q_\alpha\boldsymbol{u}_\alpha\cdot\boldsymbol{E}.\end{aligned} \tag{3}$$

Substituting Eq. (3) into Eq. (2) we obtain [20,21]

$$\partial_t E_\alpha^{\rm th} + \nabla\cdot\left(E_\alpha^{\rm th}\boldsymbol{u}_\alpha + \boldsymbol{h}_\alpha\right) = -(\boldsymbol{P}_\alpha\cdot\nabla)\cdot\boldsymbol{u}_\alpha. \tag{4}$$

Finally, from Maxwell's equations, the electromagnetic energy $E^m = \frac{1}{8\pi}(\boldsymbol{B}^2 + \boldsymbol{E}^2)$, obeys

$$\partial_t E^m + \frac{c}{4\pi}\nabla\cdot(\boldsymbol{E}\times\boldsymbol{B}) = -\boldsymbol{j}\cdot\boldsymbol{E}, \tag{5}$$

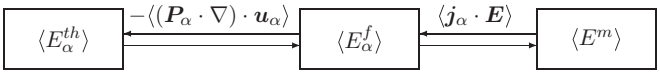

FIG. 1. Available routes for energy conversion in collisionless plasma turbulence. $\langle E_\alpha^{\rm th}\rangle$ is thermal (random) energy; $\langle E_\alpha^{f}\rangle$ is fluid flow energy; $\langle E^m\rangle$ is electromagnetic energy density. α labels each species. Brackets indicate volume average.

where $\boldsymbol{j}=\sum_\alpha n_\alpha q_\alpha \boldsymbol{u}_\alpha$ is the total electric current density. Integrating Eqs. (3), (4), and (5) over the entire volume, and invoking periodic (or isolating) boundary conditions, we find that

$$\partial_t\langle E_\alpha^{f}\rangle = \langle(\boldsymbol{P}_\alpha\cdot\boldsymbol{\nabla})\cdot\boldsymbol{u}_\alpha\rangle + \langle n_\alpha q_\alpha \boldsymbol{u}_\alpha\cdot\boldsymbol{E}\rangle, \tag{6}$$

$$\partial_t\langle E_\alpha^{\rm th}\rangle = -\langle(\boldsymbol{P}_\alpha\cdot\boldsymbol{\nabla})\cdot\boldsymbol{u}_\alpha\rangle, \tag{7}$$

$$\partial_t\langle E^{m}\rangle = -\langle\boldsymbol{j}\cdot\boldsymbol{E}\rangle, \tag{8}$$

where $\langle\cdots\rangle$ denotes a spatial average.

The above energy balance equations are elementary consequences of the Vlasov equation. From a turbulence perspective, they indicate how the cascade converts energy from one form to another, but do not include either large-scale sources or small-scale sinks. Fully accounted for are all wave particle interactions that can convert fluctuation energy into internal energy. The Vlasov system is an *ideal* model, lacking small corrections that lead to entropy production [22], so we do not address whether this conversion becomes irreversible. Theory, computations, and observations [23,24] indicate that departures from an ideal description occur at small spatial scales, e.g., at the Debye scale, and in localized regions of space associated with coherent structures [25–27]. Coherent structure formation itself is driven by ideal nonlinear couplings [28] and consequently, Vlasov channels for energy transfer are instrumental in creating the path to dissipation.

From Eq. (2), changes in particle kinetic energy are due to $\boldsymbol{j}_\alpha\cdot\boldsymbol{E}$ where the electric current density of species α is $\boldsymbol{j}_\alpha = n_\alpha q_\alpha \boldsymbol{u}_\alpha$. This term contributes to Eq. (6), but not Eq. (7). Therefore all work done on particles by the electromagnetic field changes only the particle *fluid* energy. Accordingly, from Eq. (7), the random component of particle energy is not directly modified by $\boldsymbol{j}_\alpha\cdot\boldsymbol{E}$. Instead, changes of random energy take place only through the term $(\boldsymbol{P}_\alpha\boldsymbol{\nabla})\cdot\boldsymbol{u}_\alpha$, which exchanges energy between the fluid kinetic energy E_α^{f} of species α and the thermal (random) energy $E_\alpha^{\rm th}$ of the same species.

To emphasize these distinct roles, the channels of energy conversion are shown in Fig. 1. The pressure tensor is usefully decomposed into the (isotropic) scalar p that remains when collisions are present, and a deviatoric part Π_{ij} that may be large for low collisionality plasmas. Accordingly, the pressure interaction is

$$\begin{aligned}-(\boldsymbol{P}\cdot\boldsymbol{\nabla})\cdot\boldsymbol{u} &= -p\delta_{ij}\partial_j u_i - (P_{ij}-p\delta_{ij})\partial_j u_i\\ &= -p\theta - \Pi_{ij}D_{ij},\end{aligned} \tag{9}$$

where $p=\frac{1}{3}P_{ii}$, $\Pi_{ij}=P_{ij}-p\delta_{ij}$, $\theta=\boldsymbol{\nabla}\cdot\boldsymbol{u}$, and $D_{ij}=\frac{1}{2}(\partial_i u_j+\partial_j u_i)-\frac{1}{3}\theta\delta_{ij}$. The term involving p is the *pressure dilatation*, familiar in ordinary fluid and magnetohydrodynamics (MHD), and found to be important in compressible cascades [29–32]. We refer to the term involving the traceless tensor $\boldsymbol{\Pi}$ as the "*Pi-D*" interaction, emphasizing that we treat it in the general case here, evaluating it directly from numerical simulations, without invoking collisional closures [33]. In collisional cases it is possible to find a closure relating *Pi-D* term to velocity gradients, so that this term is replaced by viscosity terms. Consequently, *Pi-D* can be viewed as "collisionless viscosity."

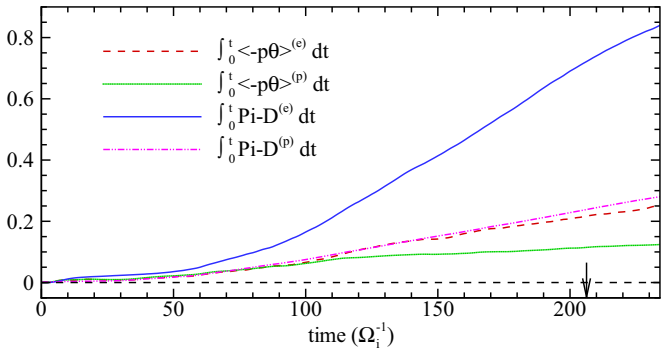

FIG. 2. Cumulative time-integrated values of *pressure dilatation* and *Pi-D* internal energy-producing terms for protons and electrons. Arrow indicates time of detailed analysis. Slopes are proportional to corresponding dissipation rates.

To demonstrate the relative importance of these energy transfer channels, we employ a kinetic simulation using the P3D code [34]. We note that the particle-in-cell (PIC) algorithm includes numerical limitations (including irreversible dissipation) related to finite particle number. While these associated departures from pure Vlasov solutions scale in a physically reasonable way [35], a direct Vlasov solution would be preferable, but at the present time is computationally prohibitive [36] for large system sizes. A 2.5-dimensional $L\times L$ periodic geometry, with two-dimensional wave vectors and three-dimensional velocity and magnetic field vectors enables a high spatial resolution, 8192^2 grid points, and a large system size $L=102.4d_i$. The simulation used 300 particles of each species per cell and $\sim 4\times 10^{10}$ total particles. The ion to electron mass ratio is $m_i/m_e=25$. The ion beta is $\beta_i=0.1$; and the electron beta is $\beta_e=0.1$; the uniform magnetic field is $B_0=5$ directed out of the plane. All quantities are normalized to reference values: density $n_r=1$, magnetic field $B_r=1$, and proton mass $m_i=1$. Length is normalized to the ion inertial length d_i, and velocity to the Alfvén speed $v_{Ar}=B_r/(4\pi m_i n_r)^{1/2}$. The run shown here is a decaying initial value problem, starting with uniform density ($n_0=1$) and temperature ($T_0=1.25$). Initial velocity and magnetic fluctuations are transverse to B_0, with a prescribed spectrum for wave numbers $2\leqslant|\boldsymbol{k}|\leqslant 4$ (see [37] for details). The data were low-pass filtered to remove noise.

Strength of energy channels. The time histories of (integrated) global volume averages of pressure dilatation $-p\boldsymbol{\nabla}\cdot\boldsymbol{u}$ and the *Pi-D* interaction term $-\Pi_{ij}D_{ij}$ (separately for $\alpha=$ protons and electrons), are shown in Fig. 2. Table I shows instantaneous values of these quantities as well as the electromagnetic work $\boldsymbol{j}_\alpha\cdot\boldsymbol{E}$ at the time of analysis around $t=205\Omega_i^{-1}$, shortly after the mean-square current reaches its maximum.

One observes that the *Pi-D* term is larger than the pressure dilatation for protons and electrons. The global average of the

TABLE I. Volume-integrated quantities related energy transfer and computed from the 2.5D undriven PIC code near the time of maximum mean-square current density. Quantities listed are in the code units $v_{Ar}^3 d_i^{-1}$. Values of $\boldsymbol{j}_\alpha$ and $\boldsymbol{E}$ time averaged over an electron gyroperiod are used in computing $\langle \boldsymbol{j}_\alpha \cdot \boldsymbol{E} \rangle$ to eliminate very high frequency oscillations.

Global Average	Electrons	Protons
p-dilatation: $\langle -p\theta \rangle$	0.0018	0.00075
Pi-D: $\langle -\Pi_{ij} D_{ij} \rangle$	0.0045	0.0016
$\langle \boldsymbol{j}_\alpha \cdot \boldsymbol{E} \rangle$	0.0052	0.0016

electromagnetic work, $\boldsymbol{j}_\alpha \cdot \boldsymbol{E}$, is comparable to the *Pi-D* term for the two species, 0.0016 ($v_{Ar}^3 d_i^{-1}$) for protons and 0.0052 ($v_{Ar}^3 d_i^{-1}$) for electrons. All three terms, $-p\boldsymbol{\nabla} \cdot \boldsymbol{u}$, *Pi-D*, and $\boldsymbol{j}_\alpha \cdot \boldsymbol{E}$, can be locally + or −, with a net positive average due to a slight asymmetry of the distribution.

Coherent structures and intermittency. Activity in these energy transfer channels is distributed nonuniformly in real space. Figure 3 shows spatial contour maps of the *Pi-D* terms, separately for protons and electrons. The first thing to notice is that the larger values (of both signs) are concentrated in small scale structures. Many such concentrations are sheetlike regions along what appears to be the boundaries of interacting magnetic flux tubes. This is reminiscent of the patterns of intense electric current density in MHD [38,39] and in plasma turbulence [26]. In decaying turbulence, these are regions of enhancements of kinetic activity [40,41]. In addition, the maps of the proton term $-\Pi_{ij}^p D_{ij}^p$ and the electron term $-\Pi_{ij}^e D_{ij}^e$ are very similar in position and shape. This is reminiscent of the finding [25], that in turbulence, proton currents collapse to a few ion inertial scales, while electron scale current sheets collapse to still finer scales (e.g., d_e), often forming *inside* the proton current structures.

The spatial concentration of the *Pi-D* due to cascade provides a pathway for coherent structures to contribute to plasma dissipation, i.e., degeneration of energy in fluid scale fluctuations. Presumably transfer to still smaller scales leads

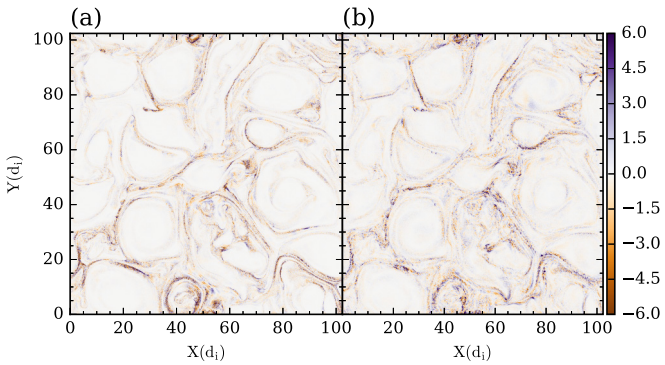

FIG. 3. Contour maps of *Pi-D* terms $-\Pi_{ij}^\alpha D_{ij}^\alpha$ for (a) electrons ($\alpha = e$) and (b) protons ($\alpha = p$) normalized to respective root mean-square values. Both display concentrations in small subvolumes, in sheetlike structures. There is remarkable similarity in proton and electron cases. Conversion between flow energy and internal energy is strong in these structures. The global average is positive corresponding to generation of internal energy.

to non-Vlasov collisional effects that provide entropy increase and heating. Here, due to the PIC algorithm, heating at small scales is due to finite particle number (see, however, [35]).

An overall view of the collisionless cascade emerges in this way: An MHD cascade creates strong current sheets that in turn generate localized small-scale vortices [42,43]. During the cascade electromagnetic work, $\boldsymbol{j} \cdot \boldsymbol{E}$, is done on particles, at locations concentrated near coherent current structures [27]. In the large Reynolds number limit, nearby vortices are stretched to planar sheetlike structures that have equal parts symmetric and antisymmetric velocity stresses. The traceless pressure tensor Π_{ij} interacts with the symmetric velocity stress [44] at these locations to distort distribution functions [40,41], producing anisotropic heating [43,45] and other kinetic effects. This also explains (see also [43]) the strong correlation between proton heating and vorticity [46,47].

The remarkable connections between coherent structures and energy conversion are further clarified by examining the spatial concentration of *Pi-D* in comparison with symmetric velocity stress, vorticity, and current density. Natural measures of these are the normalized second (tensor) invariants, for the symmetric traceless stress, $Q_D = \frac{1}{2} D_{ij} D_{ij} / \langle 2 D_{ij} D_{ij} \rangle$; for the vorticity, $Q_\omega = \frac{1}{4} \boldsymbol{\omega}^2 / \langle \boldsymbol{\omega}^2 \rangle$ and for the mean-square total current density, $Q_j = \frac{1}{4} \boldsymbol{j}^2 / \langle \boldsymbol{j}^2 \rangle$. To portray the spatial correlations among these quantities, Fig. 4 compares the electron *Pi-D* map with contour maps of Q_D, Q_ω, and Q_j. One sees that these quantities are concentrated in very similar spatial regions. This intermittency was completely absent in the specified initial data. Therefore the observed coherent structure is a consequence of the turbulent cascade.

Conditional averages. The striking correlation seen in Fig. 4 is quantified by computing conditional averages. Figure 5 shows conditional averages of the *Pi-D* terms, the rate of production of internal energy, $-\Pi_{ij} D_{ij}$, separately for protons and electrons. The conditions are based on values of Q_D, Q_ω, and Q_j. For example, to compute $\langle -\Pi_{ij}^e D_{ij}^e | Q_j \rangle$, one averages the electron *Pi-D* including only values occurring at spatial positions at which the mean-square total electric current density (Q_j) exceeds a selected threshold. The figure confirms that, for both electrons and protons, elevated levels of $-\Pi_{ij} D_{ij}$ are found in regions with enhanced vorticity (consistent with earlier reports [43,47]) and in regions of enhanced symmetric stress. In contrast, averages of *Pi-D* conditioned on total current density remain fairly constant for protons, and slightly decrease for electrons. Note that values of *Pi-D* for protons are even more elevated in regions of large symmetric stress than in regions of large (mean-square) vorticity. These conditional variations of *Pi-D* provide important constraints on understanding mechanisms of plasma heating.

Discussion and conclusions. In this Rapid Communication we have examined new directions for studying turbulence cascade in the Vlasov-Maxwell system that describe the *ideal* dynamics of a weakly collisional plasma. In analogy to the Euler equations for ideal fluids, the Vlasov is a lossless mean-field description, describing the cascade in a large system, without reference to the collisional effects at finer spatial and temporal scales.

From the Vlasov equation, the major contributors to conversion of energy are the species-dependent $\boldsymbol{j} \cdot \boldsymbol{E}$, the species-

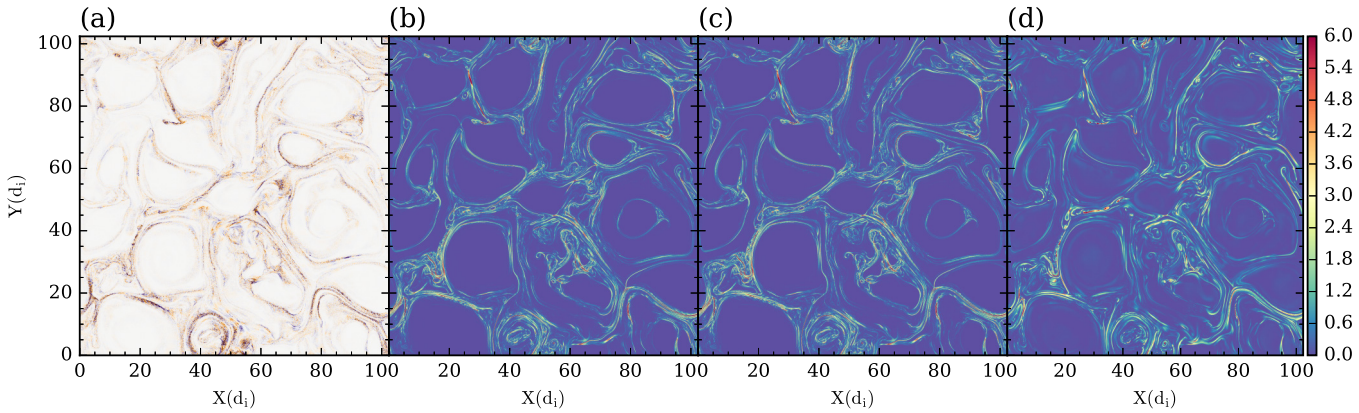

FIG. 4. Left to right: *Pi-D* term for electrons; Q_D and Q_ω for electron flow, and Q_j from total current density.

dependent pressure dilatation $-p\nabla\cdot\boldsymbol{u}$, and the species-dependent "*Pi-D*" term $-\Pi_{ij}D_{ij}$. The *Pi-D* terms and pressure dilatation are the only couplings in the Vlasov-Maxwell system that can generate internal energy. Accordingly, the electromagnetic work terms only exchange energy with the fluid flow energy of the various species. This elementary property of the Vlasov system has evidently not been fully appreciated as a guideline for analysis of collisionless turbulence.

Of some significance, is the fact that the contributions of the *off-diagonal terms* of the pressure tensor, through the *Pi-D* terms, are found empirically to be larger than the contributions of the (diagonal) pressure dilatation term. In addition, we find that all pressure-stress terms, including *Pi-D*, become highly localized in space due to turbulent cascade, similar to the localization found previously for electromagnetic work on particles ($\boldsymbol{j}\cdot\boldsymbol{E}$), for the vorticity, and for electric current density. A further remarkable result is that several types of coherent structures occur in similar but not identical [43] positions and patterns in space. This implies that a strong dynamical coupling exists between energy conversion and both velocity and magnetic stress tensors, even in collisionless plasmas.

The results presented here suggest an emerging picture of the energy channels that lead to dissipation in low collisionality plasma turbulence: The larger MHD-scale nonlinearities are reasonably well understood [5,32,48] and drive scale-to-scale transfer, with a net transfer to small scales. As the cascade transfers energy to smaller scales, the dynamics progressively generates coherent structures [26], as observed here. Within these structures, one finds a concentration of all channels of energy conversion. Magnetic energy, at scales approaching proton kinetic scales, is converted into both proton flows and electron flows. This process is highly associated with local current density [24,26]. Pressure dilatation and pressure-symmetric stress interactions (pressure dilatation and *Pi-D*) take over at that point and convert energy from these flows into internal energy. Vorticity distorts the distribution functions [36,40,41,43,45] while pressure-symmetric stress interactions convert these flows into internal energy.

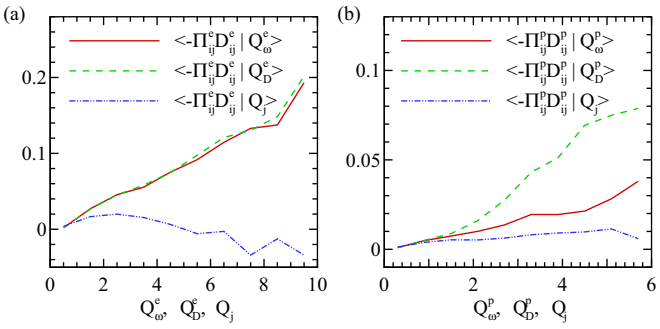

FIG. 5. Conditional averages of the (a) electron *Pi-D* term and (b) proton *Pi-D* term. In both cases the conversion of internal energy by the *Pi-D* terms is concentrated in coherent structures generated by the turbulence. For electrons, vorticity and symmetric stress are both important. For protons, symmetric stress is the most important; for signed vorticity effect, see [43,47].

We note that this description of the pathways to dissipation in a Vlasov plasma appears to be quite general, and may, presumably, be applied to whistler or kinetic Alfvén wave turbulence [18,23], or more general cases. The sequence of energy transfer channels described above is also reminiscent of the structure of heating mechanisms invoked in reconnection studies [49,50]. However, the approach suggested here does not require a focus on any particular wave or mechanism.

These results provide guidance for pursuing additional study of dissipation in space and astrophysical turbulence. The statistical properties of these new types of correlated intermittent structures warrant further study, while scale decomposition [6,16,31,32] of energy transfer and exchange will reveal cascade properties in the kinetic range of plasma turbulence. A deeper understanding of energy transfer channels will be useful in interpreting results from space missions, including the ongoing MMS and Cluster missions, the upcoming Solar Probe Plus and Solar Orbiter mission, and the planned THOR mission.

Acknowledgments. This research is supported in part by NSF AGS-1063439, AGS-1156094 (SHINE), AGS-1460130 (SHINE), the Parker Solar Probe science team (ISIS/SWRI project subcontract D99031L), and by NASA Grants No. NNX14AI63G (Heliophysics Grandchallenge Theory) and No. NNX14AC39G (MMS Theory and Modeling). We would like to acknowledge high-performance computing support from Yellowstone (ark:/85065/d7wd3xhc) provided by NCAR's Computational and Information Systems Laboratory, sponsored by the National Science Foundation. Y.Y. is

supported by a Visiting Scholar program at Delaware from the China Scholarship Council. M.W. is supported by NSFC Grant No. 11672123. We thank Colby Haggerty for assistance with preparing the data.

[1] A. S. Monin and A. M. Yaglom, *Statistical Fluid Mechanics* (MIT Press, Cambridge, MA, 1971, 1975), Vols. 1 and 2.
[2] D. Biskamp, *Magnetohydrodynamic Turbulence* (Cambridge University Press, Cambridge, UK, 2003).
[3] R. H. Kraichnan and D. C. Montgomery, Rep. Prog. Phys. **43**, 547 (1980).
[4] Y. Zhou, W. H. Matthaeus, and P. Dmitruk, Rev. Mod. Phys. **76**, 1015 (2004).
[5] M. K. Verma, Phys. Rep. **401**, 229 (2004).
[6] A. Alexakis, P. D. Mininni, and A. Pouquet, New J. Phys. **9**, 298 (2007).
[7] H. Politano and A. Pouquet, Geophys. Res. Lett. **25**, 273 (1998).
[8] L. Sorriso-Valvo, R. Marino, V. Carbone, A. Noullez, F. Lepreti, P. Veltri, R. Bruno, B. Bavassano, and E. Pietropaolo, Phys. Rev. Lett. **99**, 115001 (2007).
[9] B. T. MacBride, C. W. Smith, and M. A. Forman, Astrophys. J. **679**, 1644 (2008).
[10] Filamentation in velocity space, analogous to real-space turbulence cascade, is a better studied feature of Vlasov plasma dynamics [12,51,52], but is not the focus of interest here.
[11] S. Boldyrev, K. Horaites, Q. Xia, and J. C. Perez, Astrophys. J. **777**, 41 (2013).
[12] A. A. Schekochihin, S. C. Cowley, W. Dorland, G. W. Hammett, G. G. Howes, G. G. Plunk, E. Quataert, and T. Tatsuno, Plasma Phys. Controlled Fusion **50**, 124024 (2008).
[13] A. B. Navarro, P. Morel, M. Albrecht-Marc, D. Carati, F. Merz, T. Görler, and F. Jenko, Phys. Rev. Lett. **106**, 055001 (2011).
[14] G. G. Plunk and T. Tatsuno, Phys. Rev. Lett. **106**, 165003 (2011).
[15] B. Teaca, A. B. Navarro, and F. Jenko, Phys. Plasmas **21**, 072308 (2014).
[16] P. Morel, A. B. Navarro, M. Albrecht-Marc, D. Carati, F. Merz, T. Görler, and F. Jenko, Phys. Plasmas **19**, 012311 (2012).
[17] F. Sahraoui, M. L. Goldstein, G. Belmont, P. Canu, and L. Rezeau, Phys. Rev. Lett. **105**, 131101 (2010).
[18] S. Saito, S. P. Gary, H. Li, and Y. Narita, Phys. Plasmas **15**, 102305 (2008).
[19] S. Boldyrev and J. C. Perez, Astrophys. J. **758**, L44 (2012).
[20] S. I. Braginskii, Rev. Plasma Phys. **1**, 205 (1965).
[21] J. P. Freidberg, Rev. Mod. Phys. **54**, 801 (1982).
[22] T. Tatsuno, W. Dorland, A. A. Schekochihin, G. G. Plunk, M. Barnes, S. C. Cowley, and G. G. Howes, Phys. Rev. Lett. **103**, 015003 (2009).
[23] G. G. Howes, S. C. Cowley, W. Dorland, G. W. Hammett, E. Quataert, and A. A. Schekochihin, J. Geophys. Res. **113**, A05103 (2008).
[24] M. Wan, W. H. Matthaeus, V. Roytershteyn, T. N. Parashar, P. Wu, and H. Karimabadi, Phys. Plasmas **23**, 042307 (2016).
[25] H. Karimabadi, V. Roytershteyn, M. Wan, W. H. Matthaeus, W. Daughton, P. Wu, M. Shay, B. Loring, J. Borovsky, E. Leonardis, S. C. Chapman, and T. K. M. Nakamura, Phys. Plasmas **20**, 012303 (2013).
[26] M. Wan, W. H. Matthaeus, H. Karimabadi, V. Roytershteyn, M. Shay, P. Wu, W. Daughton, B. Loring, and S. C. Chapman, Phys. Rev. Lett. **109**, 195001 (2012).
[27] M. Wan, W. H. Matthaeus, V. Roytershteyn, H. Karimabadi, T. Parashar, P. Wu, and M. Shay, Phys. Rev. Lett. **114**, 175002 (2015).
[28] M. Wan, S. Oughton, S. Servidio, and W. H. Matthaeus, Phys. Plasmas **16**, 080703 (2009).
[29] G. L. Eyink, Physica D **207**, 91 (2005).
[30] G. L. Eyink and H. Aluie, Phys. Fluids **21**, 115107 (2009).
[31] H. Aluie, S. Li, and H. Li, Astrophys. J. Lett. **751**, L29 (2012).
[32] Y. Yang, Y. Shi, M. Wan, W. H. Matthaeus, and S. Chen, Phys. Rev. E **93**, 061102 (2016).
[33] R. D. Hazeltine and F. L. Waelbroeck, *The Framework of Plasma Physics* (Westview Press, Boulder, 2004).
[34] A. Zeiler, D. Biskamp, J. F. Drake, B. N. Rogers, M. A. Shay, and M. Scholer, J. Geophys. Res.: Space Phys. **107**, 1230 (2002).
[35] D. Montgomery and C. W. Nielson, Phys. Fluids **13**, 1405 (1970).
[36] S. Servidio, F. Valentini, D. Perrone, A. Greco, F. Califano, W. H. Matthaeus, and P. Veltri, J. Plasma Phys. **81**, 325810107 (2015).
[37] P. Wu, M. Wan, W. H. Matthaeus, M. A. Shay, and M. Swisdak, Phys. Rev. Lett. **111**, 121105 (2013).
[38] W. H. Matthaeus and D. Montgomery, Ann. N.Y. Acad. Sci. **357**, 203 (1980).
[39] V. Carbone, P. Veltri, and A. Mangeney, Phys. Fluids **2**, 1487 (1990).
[40] S. Servidio, F. Valentini, F. Califano, and P. Veltri, Phys. Rev. Lett. **108**, 045001 (2012).
[41] A. Greco, F. Valentini, S. Servidio, and W. H. Matthaeus, Phys. Rev. E **86**, 066405 (2012).
[42] W. H. Matthaeus, Geophys. Res. Lett. **9**, 660 (1982).
[43] T. N. Parashar and W. H. Matthaeus, Astrophys. J. **832**, 57 (2016).
[44] D. D. Sarto, F. Pegoraro, and F. Califano, Phys. Rev. E **93**, 053203 (2016).
[45] S. Servidio, K. T. Osman, F. Valentini, D. Perrone, F. Califano, S. Chapman, W. H. Matthaeus, and P. Veltri, Astrophys. J. Lett. **781**, L27 (2014).
[46] J. D. Huba, Geophys. Res. Lett. **23**, 2907 (1996).
[47] L. Franci, P. Hellinger, L. Matteini, A. Verdini, and S. Landi, in *Solar Wind 14: Proceedings of the Fourteenth International Solar Wind Conference, Weihai, China*, edited by L. Wang, R. Bruno, E. Möbius, A. Voulida, and G. Zank, AIP Conf. Proc No. 1720 (AIP, Melville, NY, 2016), p. 040003.
[48] H. Aluie and G. L. Eyink, Phys. Rev. Lett. **104**, 081101 (2010).
[49] J. F. Drake, M. Swisdak, T. D. Phan, P. A. Cassak, M. A. Shay, S. T. Lepri, R. P. Lin, E. Quataert, and T. H. Zurbuchen, J. Geophys. Res.: Space Phys. **114**, A05111 (2009).
[50] C. C. Haggerty, M. A. Shay, J. F. Drake, T. D. Phan, and C. T. McHugh, Geophys. Res. Lett. **42**, 9657 (2015).
[51] T. Armstrong and D. Montgomery, J. Plasma Phys. **1**, 425 (1967).
[52] C. Z. Cheng and G. Knorr, J. Comput. Phys. **22**, 330 (1976).